









## Ephemeral Surface Chlorophyll Enhancement at the New England Shelf Break Driven by Ekman Restratification

Hilde Oliver<sup>1</sup> , Weifeng Gordon Zhang<sup>1</sup> , Kevin M. Archibald<sup>1</sup> , Andrew J. Hirzel<sup>1</sup> , Walker O. Smith Jr<sup>2,3</sup> , Heidi M. Sosik<sup>1</sup> , Rachel H. R. Stanley<sup>4</sup> , and Dennis J. McGillicuddy Jr<sup>1</sup> 

<sup>1</sup>Woods Hole Oceanographic Institution, Woods Hole, MA, USA, <sup>2</sup>Virginia Institute of Marine Science, College of William & Mary, Gloucester Point, VA, USA, <sup>3</sup>School of Oceanography, Shanghai Jiao Tong University, Shanghai, China, <sup>4</sup>Department of Chemistry, Wellesley College, Wellesley, MA, USA

### Key Points:

- Spring enhancements of surface chlorophyll at the New England shelf break are short-lived and thus are not visible in seasonal means
- Surface chlorophyll enhancements are associated with offshore displacement of the upper part of the shelf-break front in spring
- Upfront wind stress increases before shelf-break chlorophyll enhancements, suggesting Ekman restratification to be the driving mechanism

### Supporting Information:

Supporting Information may be found in the online version of this article.

### Correspondence to:

H. Oliver,  
[holiver@whoi.edu](mailto:holiver@whoi.edu)

### Citation:

Oliver, H., Zhang, W. G., Archibald, K. M., Hirzel, A. J., Smith, W. O. Jr, Sosik, H. M., et al. (2022). Ephemeral surface chlorophyll enhancement at the New England shelf break driven by Ekman restratification. *Journal of Geophysical Research: Oceans*, 127, e2021JC017715. <https://doi.org/10.1029/2021JC017715>

Received 23 JUN 2021  
Accepted 22 DEC 2021

**Abstract** The Mid-Atlantic Bight (MAB) hosts a large and productive marine ecosystem supported by high phytoplankton concentrations. Enhanced surface chlorophyll concentrations at the MAB shelf-break front have been detected in synoptic measurements, yet this feature is not present in seasonal means. To understand why, we assess the conditions associated with enhanced surface chlorophyll at the shelf break. We employ in-situ and remote sensing data, and a 2-dimensional model to show that Ekman restratification driven by upfront winds drives ephemerally enhanced chlorophyll concentrations at the shelf-break front in spring. Using 8-day composite satellite-measured surface chlorophyll concentration data from 2003–2020, we constructed a daily running mean (DRM) climatology of the cross-shelf chlorophyll distribution for the northern MAB region. While the frontal enhancement of chlorophyll is apparent in the DRM climatology, it is not captured in the seasonal climatology due to its short duration of less than a week. In-situ measurements of the frontal chlorophyll enhancement reveal that chlorophyll is highest in spring when the shelf-break front slumps offshore from its steep wintertime position causing restratification in the upper part of the water column. Several restratification mechanisms are possible, but the first day of enhanced chlorophyll at the shelf break corresponds to increasing upfront winds, suggesting that the frontal restratification is driven by offshore Ekman transport of the shelf water over the denser slope water. The 2-dimensional model shows that upfront winds can indeed drive Ekman restratification and alleviate light limitation of phytoplankton growth at the shelf-break front.

**Plain Language Summary** The ocean south of New England contains high concentrations of phytoplankton that form the base of the marine food web and provide critical support to the region's fisheries. The offshore edge of the relatively shallow continental shelf, the shelf break, is the boundary between the cooler and fresher water on the continental shelf (shelf water) and the warmer and saltier water offshore (slope water). This water boundary at the shelf break is thought to support high chlorophyll concentrations. Enhanced shelf-break chlorophyll concentrations are not always present, however. We use data from satellites, ships, gliders, and moorings to determine what drives the episodically enhanced surface shelf-break chlorophyll concentrations. We find that the shelf-break surface enhancements of chlorophyll concentrations are short-lived events, and are associated with periods when the shelf-slope water interface slumps, as a surface layer of the lighter shelf water moves over the denser slope water. This process creates a shallow surface layer that has ample light to support photosynthesis. Both data and a computational model show that eastward winds are the primary driver of the episodic frontal slumping and localized enhanced surface chlorophyll.

## 1. Introduction

The Mid-Atlantic Bight (MAB) region of the U.S. northeast continental shelf is home to a large and highly productive marine ecosystem (O'Reilly & Busch, 1984; O'Reilly et al., 1987), and an important region for commercial fisheries (Orphanides & Magnusson, 2007; Podestá et al., 1993). Phytoplankton concentrations and primary productivity vary substantially across the MAB. High phytoplankton biomass is often associated with the colder, fresher shelf water, while more oligotrophic conditions are associated with the warmer and saltier slope water offshore of the shelf break (e.g., Xu et al., 2011; Yoder et al., 2002; Zhang et al., 2013). A persistent shelf-break front with isopycnals shoaling offshore (Lozier & Reed, 2005) serves as the boundary between shelf water and slope water (e.g., Fratantoni, 2003; Linder & Gawarkiewicz, 1998). The location and orientation of the shelf-break

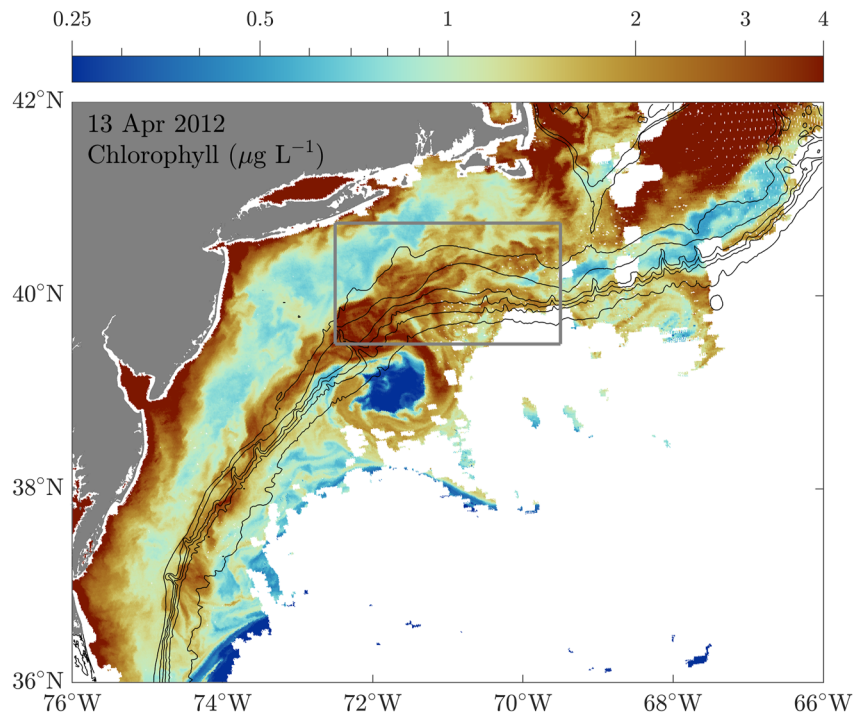


**Figure 1.** Example snapshot of enhanced chlorophyll at the shelf break, depth contours at 75, 100, 200, 500, 1,000, and 2,000 m. The gray box indicates the geographic boundaries of the map shown in Figure 3. Note the log color axis scale.

front can vary considerably. In winter, the vertical structure of the front is steep with condensed isopycnals, while in summer the front is gently sloped with strong stratification in the upper layer (Linder & Gawarkiewicz, 1998).

Sporadically enhanced chlorophyll concentrations at the shelf-break front have been detected by satellite and shipboard measurements (Figure 1; Marra et al., 1982; Ryan, Yoder, Cornillon, et al., 1999). A variety of nutrient-supplying upwelling processes have been suggested to take place at the front, including an onshore flow driven by the along-shelf pressure gradient force (Zhang et al., 2011), along-isopycnal upwelling driven by convergence within the bottom boundary layer (Chapman & Lentz, 1994; Gawarkiewicz & Chapman, 1992; Linder et al., 2004), and vertical transport induced by frontal meandering (Zhang & Gawarkiewicz, 2015). Frontal chlorophyll enhancement is not always present, however (Hales et al., 2009), and is not visible in seasonal chlorophyll climatologies (e.g., Zhang et al., 2013). The absence of a mean chlorophyll enhancement at the shelf break, given the variety of potential upwelling mechanisms, has presented a critical gap in our understanding of the bio-physical interactions governing this economically important marine ecosystem (Sherman et al., 1996). The central question is two-pronged: (a) what drives the enhanced surface chlorophyll when it occurs at the shelf break, and (b) why is it not detected in the seasonal means?

Here, we explore the timing and duration of chlorophyll enhancements at the New England shelf break using satellite-based estimates of surface chlorophyll *a* concentrations made from ocean color measurements. To understand the environmental conditions that give rise to these enhancements, we use shipboard data collected in mid-to-late April 2018 and data from the Oceans Observatories Initiative (OOI) Coastal Pioneer Array (Gawarkiewicz & Plueddemann, 2020; Trowbridge et al., 2019), which we then test with 2-dimensional coupled physical-biogeochemical simulations.

## 2. Materials and Methods

### 2.1. Satellite Chlorophyll *a*

We analyzed Moderate Resolution Imaging Spectroradiometer (MODIS) Aqua 8-day composite 1-km surface chlorophyll *a* data (OC3 algorithm) from 2003 to 2020 to identify times of higher surface chlorophyll concentrations at the shelf break than neighboring slope and shelf region. While there is frequently heavy cloud cover

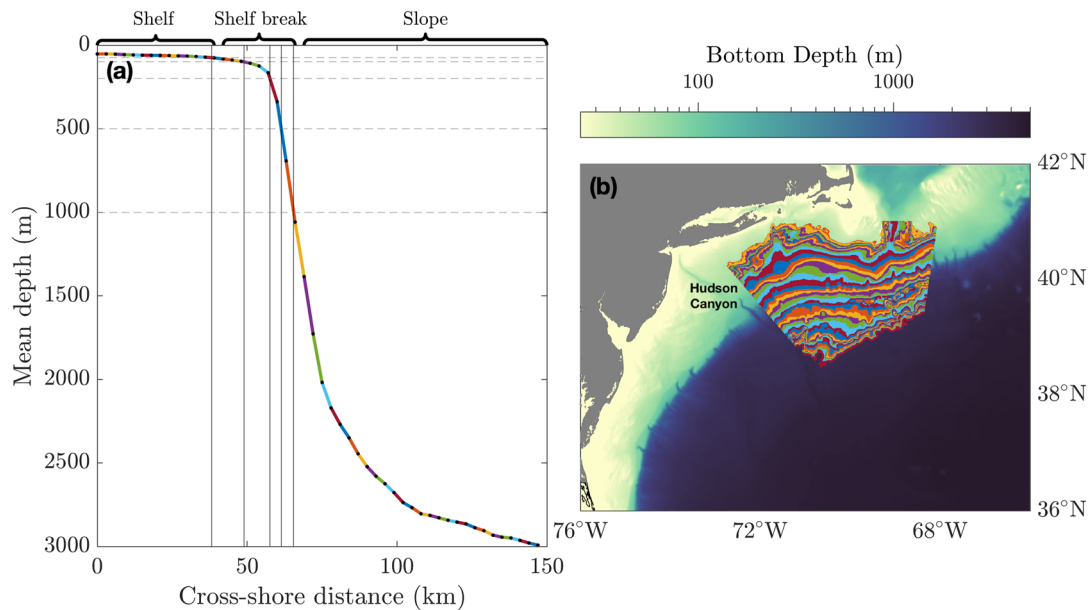


**Figure 2.** (a) Mean cross-shelf bathymetric profile, partitioned into the 51 depth bins (equally spaced 3 km apart), with the 75, 100, 200, 500, and 1,000 m isobaths identified by vertical and horizontal lines, and bins identified as belonging to the shelf, shelf break, and slope sections; (b) geographic distribution of the 51 depth bins, selected by dividing the mean cross-shelf profile in (a) into 3-km segments. Note that bins from the shelf break will cover a larger depth range than those on the shelf or slope. For clarity a repeating color map is utilized in both (a) and (b) for each depth bin. Note the log color axis scale in (b).

over the region, the 8-day composite product can provide nearly-continuous chlorophyll data over the shelf-break area. The 8-day composite chlorophyll fields are available daily, and are an effective 8-day moving average of chlorophyll in each 1-km pixel. We therefore henceforth refer to the 8-day chlorophyll composites as daily running means (DRM).

We analyze chlorophyll distributions from the Hudson Canyon to 68°W, and from a bottom depth of 50–3,000 m (Figure 2). Individual ocean color images showing enhanced chlorophyll along the entire MAB shelf break are relatively rare, likely due to cloud cover or extensive along- and cross-front variability in chlorophyll concentrations. To account for spatial and temporal variability and to achieve an along-shelf mean picture of the chlorophyll distribution, we averaged chlorophyll concentrations in the along-shelf direction. As the frontal flow in the shelf break region is often topographically steered, the averaging was carried out using bottom depth as the cross-shelf coordinate. The procedure of the averaging is as follows: (a) the mean cross-shelf bathymetric profile within the range of 50–3,000 m was discretized into 3 km intervals, which gives a total of 51 bottom depth bins (Figure 2a); (b) for each day, the surface DRM chlorophyll value at each pixel was then placed in a depth bin according to the water depth (Figure 2b); and (c) all chlorophyll values in each depth bin were then averaged to obtain the mean chlorophyll concentration of that bin. The distribution of the bin-averaged chlorophyll concentration against the mean cross-shelf distance of the depth bins gives the along-shelf-averaged cross-shelf distribution of surface chlorophyll concentration of the 8-day window.

## 2.2. Shipboard Data

From 16–29 April 2018, R/V Neil Armstrong cruise AR29 sampled repeatedly across the New England shelf break along 70.83°W (Figure 3), centered between the moorings installed at the OOI Coastal Pioneer Array. The objective of cruise AR29 was to investigate the mechanisms controlling primary productivity at the shelf-break front, as part of the interdisciplinary Shelf-break Productivity Interdisciplinary Research Operation at the Pioneer Array (SPIROPA). From 3–12 April 2018, R/V Neil Armstrong cruise AR28B also conducted cross-shelf CTD transects at 70.83°W, which provided information about the conditions preceding the SPIROPA cruise.

During AR29, a Video Plankton Recorder II (VPR, from SeaScan Inc.) was towed behind the ship for high-resolution surveys of temperature, salinity, and fluorescence across the shelf break. The VPR consists of a towed body, and is equipped with a Seabird Electronics Inc. SBE 49 FastCat CTD, SBE 43 oxygen sensor, ECO FLNTU-4050

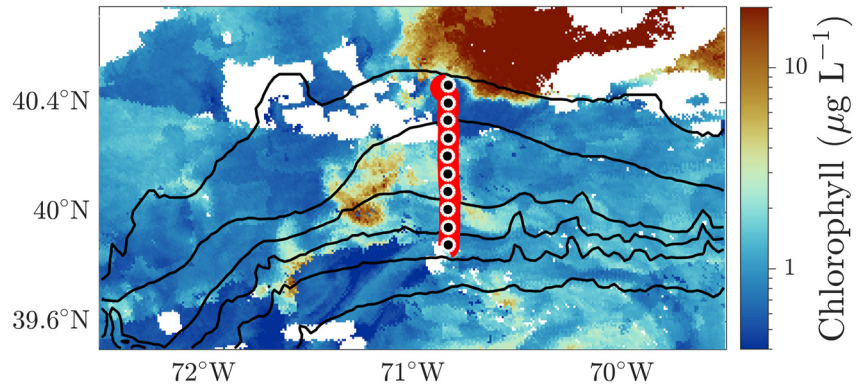


**Figure 3.** Map of 18 April, video plankton recorder (VPR) tow (red line) and 19 April, CTD Transect 5 cast locations (black circles) overlaid on April 18 DRM chlorophyll from MODIS-Aqua. Black circles represent Stations A5 to A14, from north to south.

fluorometer, ECO BBFL2-123 ECO Triplet, Biospherical Instruments Inc. QCP-200L PAR sensor, and a synchronized video camera and xenon strobe (Davis et al., 2005). The VPR was towed at 10 knots ( $5.1 \text{ m s}^{-1}$ ), undulating between 5 and up to 100 m with a vertical velocity of approximately  $1 \text{ m s}^{-1}$ . Net community production (NCP) integrated over the mixed layer was calculated for the VPR transect from  $\text{O}_2/\text{Ar}$  measured continuously (seconds-to-minutes) by an Equilibrator Inlet Mass Spectrometer (EIMS) from the ship's underway system (intake depth = 2.1 m; Smith et al., 2021). We present data from VPR Tow 1 on 18 April 2018, near the beginning of the cruise.

High-resolution underway measurements of phytoplankton size structure were measured during the VPR tow with two types of cytometers. Pico- to nanoplankton ( $0.5\text{--}15 \mu\text{m}$ ) were measured with an Attune NxT flow cytometer (Thermo Fisher Scientific) and nano- to microplankton ( $7\text{--}150 \mu\text{m}$ ) were observed with an Imaging Flow-Cytobot (IFCB, McLane Research Laboratories). Images were captured based on the chlorophyll fluorescence signal of each particle. The Attune collected one 0.4-ml sample approximately every 2 min and the IFCB collected one 5-ml sample ca. every 26 min. All Attune samples within 10 min of each IFCB sample were pooled and combined with the data from a single IFCB file. Differences in sampling volume between the two instruments meant that the pooled Attune samples and the IFCB sample had approximately the same volume. Total phytoplankton biovolume concentrations for shelf water (salinity 32–34), frontal water (salinity 34–35), and slope water (salinity 35–35.5), used here as a proxy of phytoplankton biomass, were calculated by integrating over the composite particle size distributions. Biovolume concentrations from warm-core ring water (salinity  $>35.5$ ) represent a different hydrographic regime and are not included in this study.

Attune cell sizes were estimated from side angle light scattering, with side scattering observations periodically normalized to the mean side scattering signal of  $1 \mu\text{m}$  beads (Flow Check High Intensity Alignment Grade Particles, Polysciences). The normalized signals were converted to cell volume based on a calibration curve generated from 12 phytoplankton cultures ranging in size from 1 to  $20 \mu\text{m}$ , which were analyzed on the Attune and independently sized on a bead-calibrated Coulter Multisizer II (Beckman Coulter). IFCB particle sizes were estimated from images following the automated scheme described by Sosik and Olson (2007) and updated in Sosik et al. (2020), and biovolume of imaged targets was determined with the distance map algorithm of Moberg and Sosik (2012).

On 19 April 2018, CTD Transect 5 was conducted over the locations covered by the VPR in the previous day; we present the nutrient data for these ten stations (A5–A14) (Figure 3). CTD profiles were taken at each station spaced  $\sim 7 \text{ km}$  apart, and discrete seawater samples were collected using 24 10-L Niskin bottles mounted on the CTD rosette. The rosette was equipped with a SeaBird 911 CTD system, a WetLabs FLNTURTD fluorometer, a BioSpherical Instruments photosynthetically active radiation (PAR) sensor, and a WetLabs C-Star beam transmissometer. Temperature, salinity, and fluorescence were measured on all CTD casts. The interface between the shelf and slope waters is represented by the 34.5 isohaline, which largely coincides with the shelf-break front during spring (Linder & Gawarkiewicz, 1998). Nitrate, phosphate, and silicate concentrations were determined

by filtering water samples through 0.4  $\mu\text{m}$  polycarbonate filters, which were frozen in acid-washed polyethylene bottles before being run at the Woods Hole Oceanographic Institution Nutrient Analytical Facility.

VPR chlorophyll concentrations from fluorescence were estimated using the CTD fluorometer-chlorophyll calibration. CTD fluorescence ( $F_{\text{CTD}}$ ) was converted into chlorophyll  $a$  concentrations ( $\text{Chl}_{\text{CTD}}$ ) using a regression between fluorescence values and extracted chlorophyll  $a$  measurements from Niskin bottles:

$$\text{Chl}_{\text{CTD}} = 0.669 F_{\text{CTD}} + 0.027 \quad (1)$$

( $R^2 = 0.90$ , RMSE = 0.60). In turn, VPR concentrations of chlorophyll  $a$  ( $\text{Chl}_{\text{VPR}}$ ) were determined from fluorescence by regressing the calculated chlorophyll concentrations from the CTD cast immediately following the VPR tow (Cast 16 at Station A14, the southernmost station of CTD Transect 5; Figure 3) using ( $\text{Chl}_{\text{CTD}}$ ) with the fluorescence ( $F_{\text{VPR}}$ ) from the last VPR profile with a maximum depth of at least 95 m. The least squares fit used to calculate chlorophyll from VPR fluorescence was

$$\text{Chl}_{\text{VPR}} = 0.673 F_{\text{VPR}} + 0.298 \quad (2)$$

( $R^2 = 0.69$ , RMSE = 0.13).

We also estimated the potential seasonal onset of more nutrient-limited conditions in the MAB with surface nitrate data provided by the National Centers for Environmental Information in the 2018 World Ocean Database (Garcia et al., 2019). We extracted all surface nitrate measurements from 68.0–73°W, and 36.0–42.0°N where the bottom depth was between 75 and 1,000 m, a total of 640 observations from the top 15 m from 1933 to 2012 to create a 30-day moving median climatology of surface nitrate. Medians are used due to right-skewed concentrations. Only concentration data that were not flagged by World Ocean Database during quality assurances were incorporated.

### 2.3. OOI Coastal Glider Data

A set of Teledyne-Webb Slocum coastal gliders deployed at the OOI Coastal Pioneer Array monitor a broad area covering the outer continental shelf, shelf break, and Slope Sea. We used all available April glider measurements of temperature, salinity, and chlorophyll to assess the conditions associated with higher spring chlorophyll concentrations near the shelf break (7,861 vertical profiles from 2014–2020). The chlorophyll products provided by OOI are calculated from fluorescence (from WET Labs – ECO Puck FLBBBCD-SLK fluorometers); regular factory calibrations are performed on its glider fluorometers to provide consistent estimates of chlorophyll concentrations. Glider temperature and salinity data are measured by Sea-Bird – SBE Glider Payload CTDs (GP-CTD). The chlorophyll and density data were provided by different instruments, with differing time steps, so the chlorophyll data were linearly interpolated by the CTD time before analysis.

### 2.4. Surface Winds

We explored the wind conditions associated with shelf-break chlorophyll enhancements with in situ measured and reanalysis wind data. OOI Pioneer Array surface moorings are equipped with a bulk meteorological package 3 m above the surface that record meridional and zonal wind speeds. Wind speeds at offshore, central, and inshore surface moorings agree well with one another during periods of overlap (Figure S1 in Supporting Information S1). To fill gaps in individual mooring records, we generated a combined OOI buoy time series, using the mean zonal and meridional wind speeds available for each minute among the three buoys.

While the local OOI buoy measurements would be the most ideal data stream for comparison to MODIS chlorophyll in the Pioneer Array shelf-break area, the buoy meteorological time series only extends back to 2014, while MODIS-Aqua chlorophyll data extends back to 2003. Meteorological model reanalysis products, by contrast, provide wind speeds covering the period of interest; the European Centre for Medium-Range Weather Forecasts (ECMWF) ERA5 reanalysis product extends back to 1950 (Hersbach et al., 2018). We first assessed whether the trends in OOI buoy wind speed are captured in the reanalysis before comparing its trends to those of the MODIS shelf-break chlorophyll (Section 2.1). For comparison with OOI buoy winds (Inshore Buoy: 40.37°N, 70.88°W; Central Buoy: 40.13°N, 70.78°W; Offshore Buoy: 39.94°N, 70.88°W), ERA5 winds between 39.75 and 40.25°N

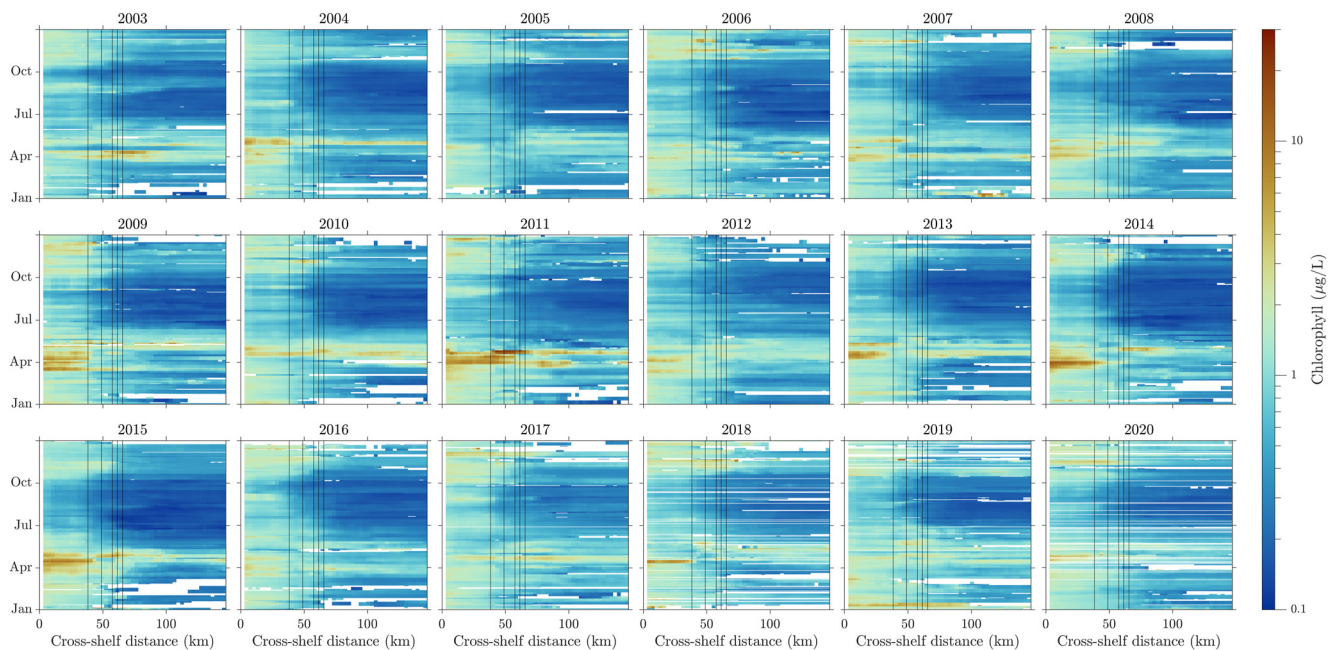


**Figure 4.** DRM depth-binned mean chlorophyll concentrations in the MAB region, from 2003–2020. Depth contours at 75, 100, 200, 500, and 1,000 m. Note the log color axis. White regions indicate cloud cover. Chlorophyll data were obtained from MODIS Aqua 8-Day 1 km composites processed at the University of Delaware.

and 69.50 and 71.50°W ( $0.25 \times 0.25$  resolution) were spatially-averaged. There is generally good agreement between the 10 m wind speeds in ERA5 winds and the OOI buoy winds (Figure S2 in Supporting Information S1).

### 2.5. 2D ROMS Configuration

We use a two-dimensional (2D; cross-shelf and vertical) configuration of the Regional Ocean Model System (ROMS; Shchepetkin & McWilliams, 2005) of the shelf-break area coupled to a nitrogen-phytoplankton-zooplankton-detritus (NPZD) model. The model spans 479 km in the cross-shelf direction with an idealized bathymetry mimicking the MAB shelf and slope seas. It is initialized with a steep front at the shelf break, using the base configuration from Zhang et al. (2011, 2013). The model has 842 grid points in the cross-shelf direction with uniform 400 m resolution in the study region and decreasing gradually to 2,400 m in the offshore region, and 60 stretched vertical layers (Figure S3 in Supporting Information S1). The 2-D across-shelf configuration is implemented via a 5-point along-shelf dimension with periodic boundary conditions. We use the same NPZD model modified from Powell et al. (2006) as used in Zhang et al. (2013), with uniform initial nitrate and phytoplankton nitrogen concentration of 5 and 1  $\mu\text{M}$ , respectively. April 2018 surface air temperatures, longwave radiation, and shortwave radiation measured at the Central Mooring (40.13°N, 70.78°W) of the OOI Pioneer Array (Gawarkiewicz & Plueddemann, 2020) are used to force the model together with idealized along-shelf winds (see below).

## 3. Results

### 3.1. MODIS-Aqua Chlorophyll Climatology

Stacking the DRM cross-shelf distributions of surface chlorophyll (Section 2.1) produces Hovmöller diagrams showing the time-evolution of the cross-shelf distribution of surface chlorophyll concentration, for each year from 2003–2020 (Figure 4). A DRM shelf-break surface chlorophyll climatology was then produced with the yearly Hovmöller diagrams presented in Figure 4. Maximum bin-averaged chlorophyll concentrations can vary widely between years, so we use the median DRM chlorophyll concentration in 2003–2020 in each depth bin.

Durations of shelf-break chlorophyll enhancements were determined with time series of the mean chlorophyll concentration at the shelf, slope, and shelf break from the yearly Hovmöller diagrams. Depth bins between the 75 and 1,000 m isobaths were categorized as the shelf-break region; those shallower were categorized as the shelf

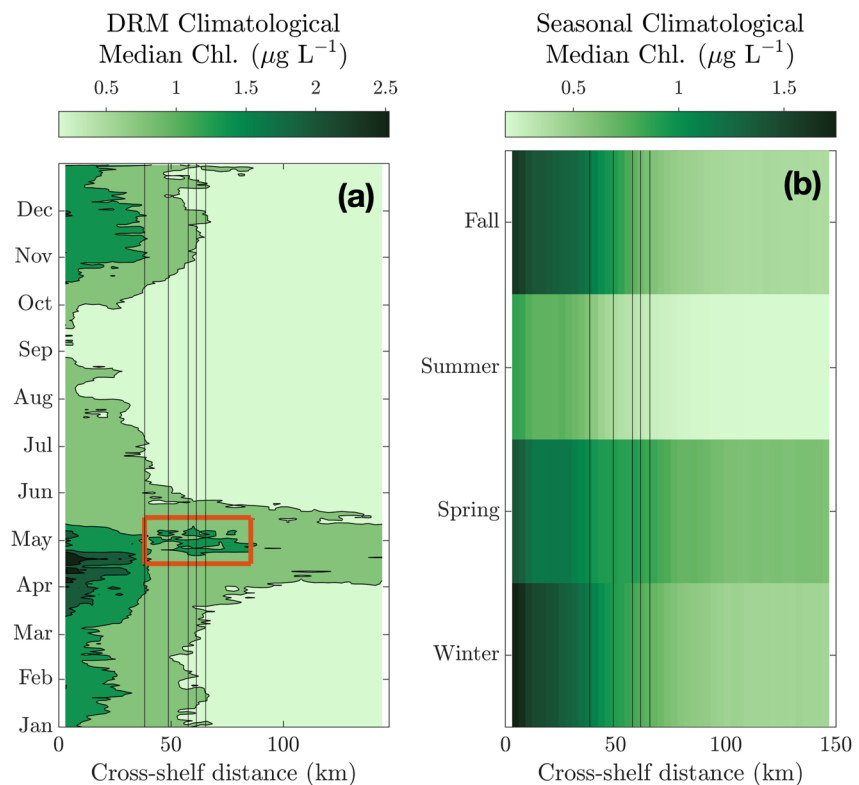


**Figure 5.** (a) DRM climatological (2003–2020) depth-binned median chlorophyll concentration in the Mid Atlantic Bight (MAB) region, with the red box indicating the period of chlorophyll enhancement at the shelf break (21 April–11 May); (b) The same as (a), but with seasonal climatological depth-binned median chlorophyll concentrations. Note the different color scales. Vertical lines show 75, 100, 200, 500, and 1,000 m depth contours.

region; and those deeper were categorized as the slope region (Figure 2a). The periods during which the mean surface chlorophyll was greater at the shelf break relative to both the shelf and slope are labeled as “enhancement days”. While the DRM chlorophyll fields provide continuous coverage over the shelf-break region, the durations of shelf-break enhancements may be underestimated (through undersampling during an enhancement) or overestimated (through undersampling before or after an enhancement) using the DRM fields. Moreover, the DRMs can underestimate the magnitude of enhancements due to temporal smearing. In any case, the DRMs are a practical means to assess spatially and temporally intermittent phenomena that are incompletely sampled due to cloud cover.

The satellite DRM chlorophyll climatology demonstrates that shelf-break chlorophyll enhancements are typically springtime features (Figure 5a). While climatological chlorophyll concentrations are higher across the shelf break for most of April and May, the period when they are enhanced relative to both the shelf and slope in the climatology is constrained to only 20 days (21 April–11 May; highlighted region in Figure 5a). The climatology shows highest chlorophyll concentrations during the inshore spring bloom beginning in mid-March, which is followed by enhanced chlorophyll at the shelf break and in the slope sea. Accordingly, periods of enhanced chlorophyll at the shelf break were identified in every year except 2004 and 2020 (Figure 6a), and many of these enhancements were concentrated within a narrow period in the spring, though some were also detected in fall and winter (Figure 6b). Generally, the shelf-break chlorophyll enhancements were short-lived, typically lasting less than a week (Figure 6c).

We also explored whether shelf-break chlorophyll enhancements were present in seasonal averages, and created a seasonal climatology by taking the median surface chlorophyll concentration in winter (January–March), spring (April–June), summer (July–September), and fall (October–December). Due to the transient quality of the surface chlorophyll enhancements, they are not expressed in the seasonal cross-shelf chlorophyll climatology (Figure 5b). While spring shelf-break chlorophyll enhancements are occasionally visible in the annual seasonal means, shelf

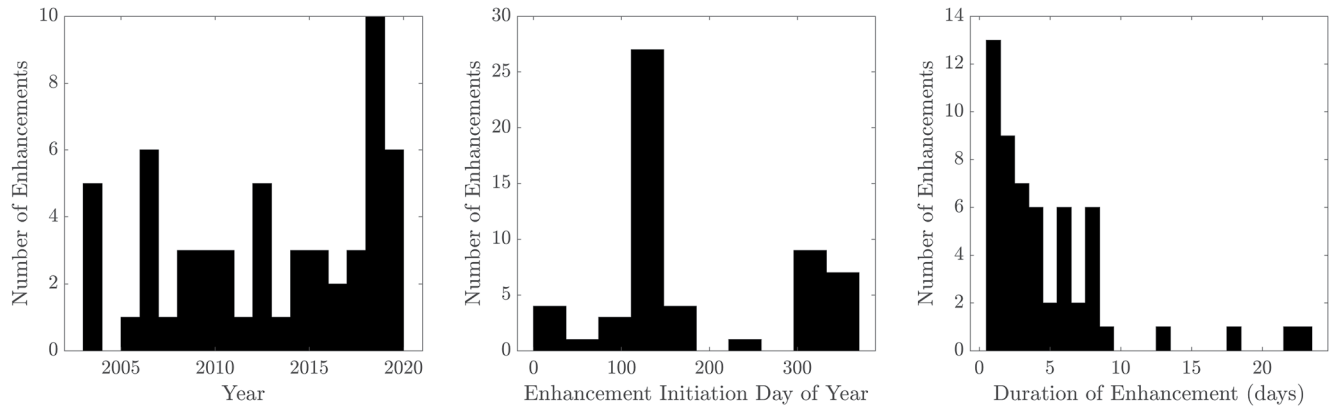


**Figure 6.** Histograms showing timing and duration of periods where shelf-break chlorophyll concentrations are enhanced relative to the shelf and slope. (a) Number of enhancements per year; (b) day of year of enhancement initiation; (c) durations of enhancements.

chlorophyll concentrations are also usually elevated in spring (excepting 2003, 2012, 2013, and 2017) and hence become indistinguishable from shelf-break enhancements in the seasonal climatology (Figure S4 in Supporting Information S1).

### 3.2. Shipboard Measurements

The conditions driving ephemeral shelf-break chlorophyll enhancements are elucidated by in-situ observations of front, shelf, and slope conditions in April 2018. On 12 April, four days before cruise AR29, the front was relatively steeply oriented (Figure 7). Within the first few days of AR29 (16–19 April), the near-surface expression of the front moved about ten kilometers offshore. The front maintained this more gently sloped configuration for a few days, until 23 April.

Elevated surface chlorophyll concentrations were measured inshore of the front during an offshore VPR tow across the shelf break on 18 April 2018 (Figure 8). Chlorophyll concentrations were highest within the ~20 m layer of cooler, fresher shelf water over the denser slope water. The shelf-slope water front was nearly horizontal beneath the chlorophyll patch, and the water column was thus more highly stratified there than elsewhere during the tow (Figures 8c and 8d). The stratification generated by the large shelf water-slope water density gradient resulted in a shallow mixed layer.

The emergence of enhanced chlorophyll associated with the onset of strengthened frontal stratification suggests that photosynthesis at the front was stimulated by the increased light levels over the shallower mixed layer (e.g., Sverdrup, 1953), not nutrients. On 19 April 2018, the 1% light depth was between 30 and 40 m (Figure 7); after restratification the mixed layer shoaled to ~20 m. Nutrient concentrations were measured over CTD Transect 5, which was conducted the day following the VPR tow along the same transect (Figure 3). Surface nitrate was always  $>4 \mu\text{M}$  (Figure 8e), suggesting nitrate-replete conditions across the shelf break, including at the front where chlorophyll was elevated. Historical measurements of surface nitrate in the MAB also show that typical MAB surface nitrate concentrations are not reduced below  $0.1 \mu\text{M}$  until mid-May (ca. Julian day 134; Figure 9). Phosphate was available in Redfield proportion to nitrate (not shown), and thus was also not limiting. Silicate concentrations were reduced to  $\sim 1 \mu\text{M}$  offshore of the front (Figure 8f), but not where elevated chlorophyll concentrations occurred. As surface nitrate concentrations were elevated across Transect 5, the emergence of elevated chlorophyll inshore of the front appears to be a result of the enhanced light availability associated with the more stratified conditions at the front.

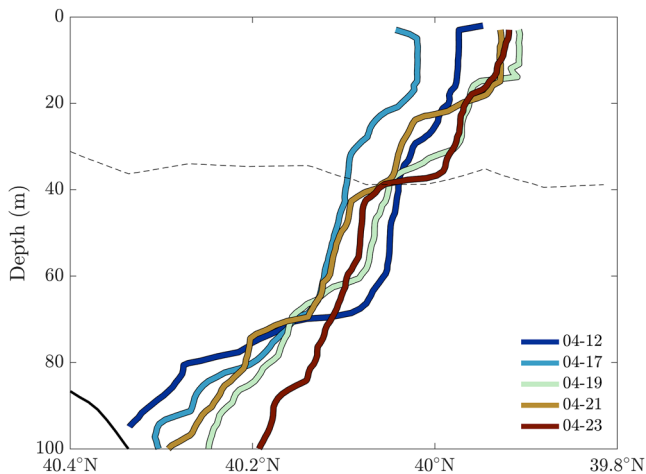


**Figure 7.** Location of the New England shelf-break front (34.5 isohaline) during in April 2018. All locations were determined from AR29 cross-shelf CTD transects at  $70.83^\circ\text{W}$ , except 12 April, which was determined from a cross-shelf CTD transect at  $70.83^\circ\text{W}$  conducted by the R/V Neil Armstrong during OOI cruise AR28B, which shortly preceded AR29. The solid black line in the bottom left corner shows the bottom depth, and the dashed black line shows the corrected 1% light depth calculated from PAR measurements from CTD casts taken on 19 April.



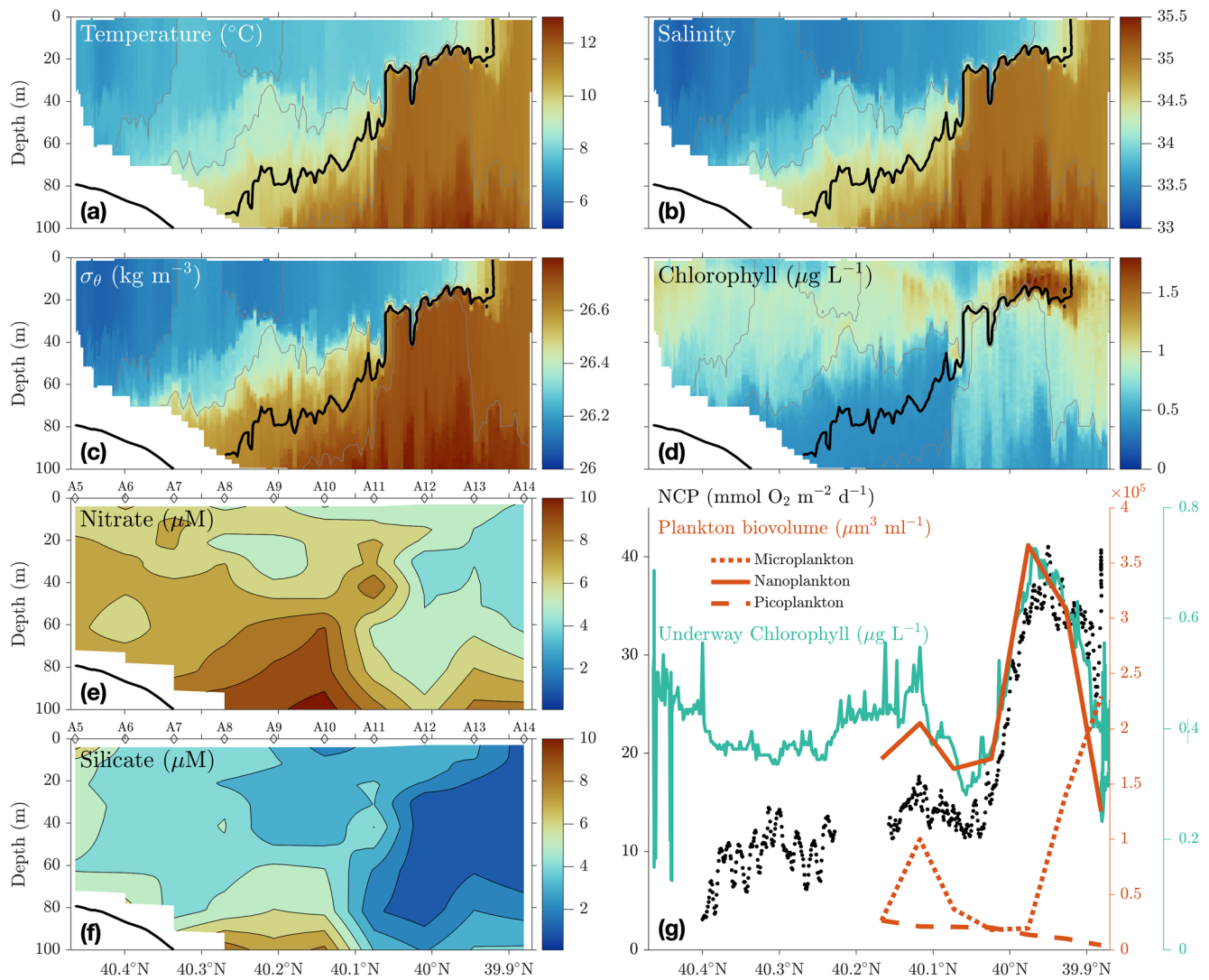


**Figure 8.** AR29 transects 18–19 April 2018. (a) Video plankton recorder (VPR) temperature ( $^{\circ}\text{C}$ ); (b) VPR salinity; (c) VPR potential density ( $\text{kg m}^{-3}$ ); (d) VPR chlorophyll estimated from fluorescence ( $\mu\text{g L}^{-1}$ ); (e) CTD Transect 5 nitrate concentrations ( $\mu\text{M}$ ); (f) CTD Transect 5 silicate concentrations ( $\mu\text{M}$ ); (g) underway measurements from the VPR tow of (1) net community production (NCP,  $\text{mmol O}_2 \text{ m}^{-2} \text{ d}^{-1}$ ), (2) microplankton, nanoplankton, and picoplankton biovolume ( $\mu\text{m}^3 \text{ ml}^{-1}$ ), and (3) underway chlorophyll ( $\mu\text{g L}^{-1}$ ). The solid black line in the bottom left corner of (a–f) shows the bottom depth.

Underway measurements conducted during the VPR tow show the enhanced frontal chlorophyll was associated with elevated NCP (Figure 8g). NCP at the front reached  $41 \text{ mmol O}_2 \text{ m}^{-2} \text{ d}^{-1}$  (equivalent to  $28 \text{ mmol C m}^{-2} \text{ d}^{-1}$  using stoichiometry from Anderson & Sarmiento, 1994), over 3 times higher than inshore of the front ( $\sim 12 \text{ mmol O}_2 \text{ m}^{-2} \text{ d}^{-1}$ ). Size fractionated biovolume from the IFCB (Figure 8g) indicates the peak in chlorophyll at the front was associated with nanoplankton, a size fraction too small to be imaged by the VPR. While chlorophyll and nanoplankton biovolume were highest at the front, total plankton biovolume concentrations at the front during the VPR tow were not higher than over the slope (Figure S5 in Supporting Information S1), as microplankton biovolume from the IFCB increased offshore of the front (Figure 8g). Analysis of IFCB and VPR images confirmed the microplankton offshore of the front were dominated by diatoms (not shown) that were apparently low in fluorometric chlorophyll. The presence of low-chlorophyll diatoms in the slope waters depleted in silicate (Figure 8f) may reflect a prior bloom unrelated to the enhanced chlorophyll and nanoplankton at the front. Later in the cruise period total biovolume was enhanced at the front relative to the shelf and slope (Figure S5 in Supporting Information S1).

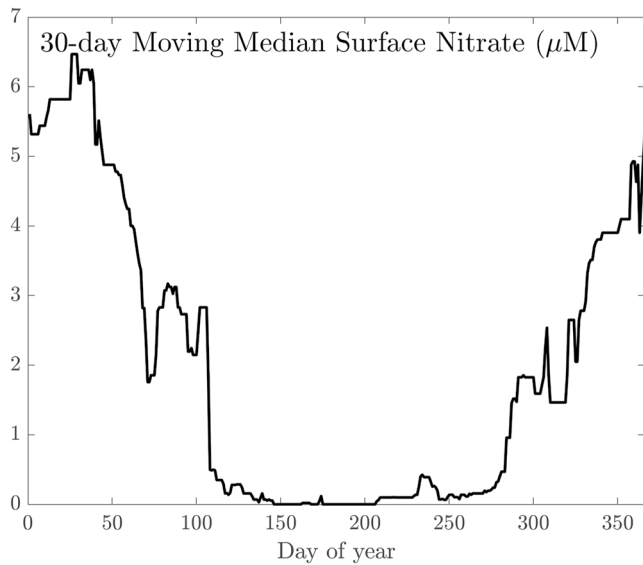


**Figure 9.** 30-day moving median of top 15 m nitrate concentrations measured in the Middle Atlantic Bight from 1932–2012 (640 observations, World Ocean Database).

### 3.3. OOI Glider Measurements

We used OOI Pioneer Array glider density and chlorophyll data to explore whether a similar frontal configuration observed during AR29 was also associated with enhanced spring shelf-break chlorophyll concentrations in other years (2014–2020, Figure 10a). In winter, the steep winter front is associated with a strong horizontal density gradient, and relatively weak vertical density gradient. As the front becomes less steep, vertical stratification increases, and a strong vertical density gradient at the front emerges (Figure 8c). A high horizontal density gradient thus indicates a location near the shelf-slope front, and a high vertical density gradient indicates high vertical stratification. We therefore interpret glider measurements with large horizontal and vertical density gradients in the near-surface layer as a place where a steep shelf-break front (with condensed isopycnals) has slumped to create strong near-surface stratification and thus a shallow surface mixed layer. The front is hence likely to be in such a configuration when a strong vertical density gradient accompanies a strong horizontal density gradient.

To assess how April chlorophyll concentrations vary with horizontal and vertical density gradients, we categorize each glider measurement in the upper water column by both its vertical density gradient  $\delta\sigma/\delta z$  and horizontal density gradient  $\delta\sigma/\delta x$ , with  $\sigma$  being potential density, averaged over 1-m depth bins. We gridded glider chlorophyll and density data by depth and distance between casts. Only glider downcasts were used because of the “V-shaped” glider trajectories, to preserve approximately uniform horizontal spacing between casts and thus more consistent horizontal density gradients.

Approximately 93,000 bins contained observations. While the calculated horizontal density gradients include variability due to internal waves, the strongest horizontal density gradients at the front are unlikely to be masked by this variability. The gridded density was then binned by the log-transformed vertical ( $\delta\sigma/\delta z$ ) and horizontal ( $\delta\sigma/\delta x$ ) density gradients. With the focus on surface enhancements, we analyzed binned density gradients over the top 30 m. Thirteen horizontal density gradient bins and 13 vertical density gradient bins were used, for a total of 169 bins. We only analyzed chlorophyll concentrations for density bins with more than 100 independent chlorophyll measurements. We assessed the chlorophyll associated with each horizontal and vertical density gradient bin using two metrics: (a) the proportion of density gradient bins where the chlorophyll reaches a concentration typical of those associated with the frontal enhancements in the binned satellite data (Figure 4;  $>2 \mu\text{g/L}$ ; “bloom bins”), and (b) the median chlorophyll concentration within each density gradient bin. Median concentrations are used because the chlorophyll distributions within each bin are right-skewed.

Chlorophyll concentrations greater than  $2 \mu\text{g L}^{-1}$  were associated with high  $\delta\sigma/\delta x$  (at the front), and low to high  $\delta\sigma/\delta z$  (a broad range of vertical density gradients) (Figure 10b). The greatest proportion of chlorophyll concentrations greater than  $2 \mu\text{g L}^{-1}$  occurred within the bin covering the highest values of  $\delta\sigma/\delta x$  and  $\delta\sigma/\delta z$ . This high  $\delta\sigma/\delta x$  and  $\delta\sigma/\delta z$  bin was also associated with higher median chlorophyll concentrations. Elevated chlorophyll concentrations in April within the top 30 m were thus most likely to occur when both horizontal and vertical density gradients were large.

The OOI glider data suggest that frontal restratification is associated with enhanced chlorophyll at the shelf-break front. We also note that higher chlorophyll can occur at the front (high  $\delta\sigma/\delta x$ ) when stratification is weak; phytoplankton blooms can also occur with the cessation of active homogenization of deep mixed layers (e.g., Ferrari et al., 2015; Taylor & Ferrari, 2011; Townsend et al., 1992).

### 3.4. Role of Upfront Winds

Upfront (eastward) winds shortly preceded the highly stratified conditions associated with enhanced shelf-break chlorophyll during AR29. On 17 April 2018, the day before VPR Tow 1, winds at the shelf break transitioned to strongly upfront (Figure S1 in Supporting Information S1), suggesting Ekman restratification as a driving mechanism for the enhanced shelf-break chlorophyll. Ekman restratification is triggered with wind forcing that

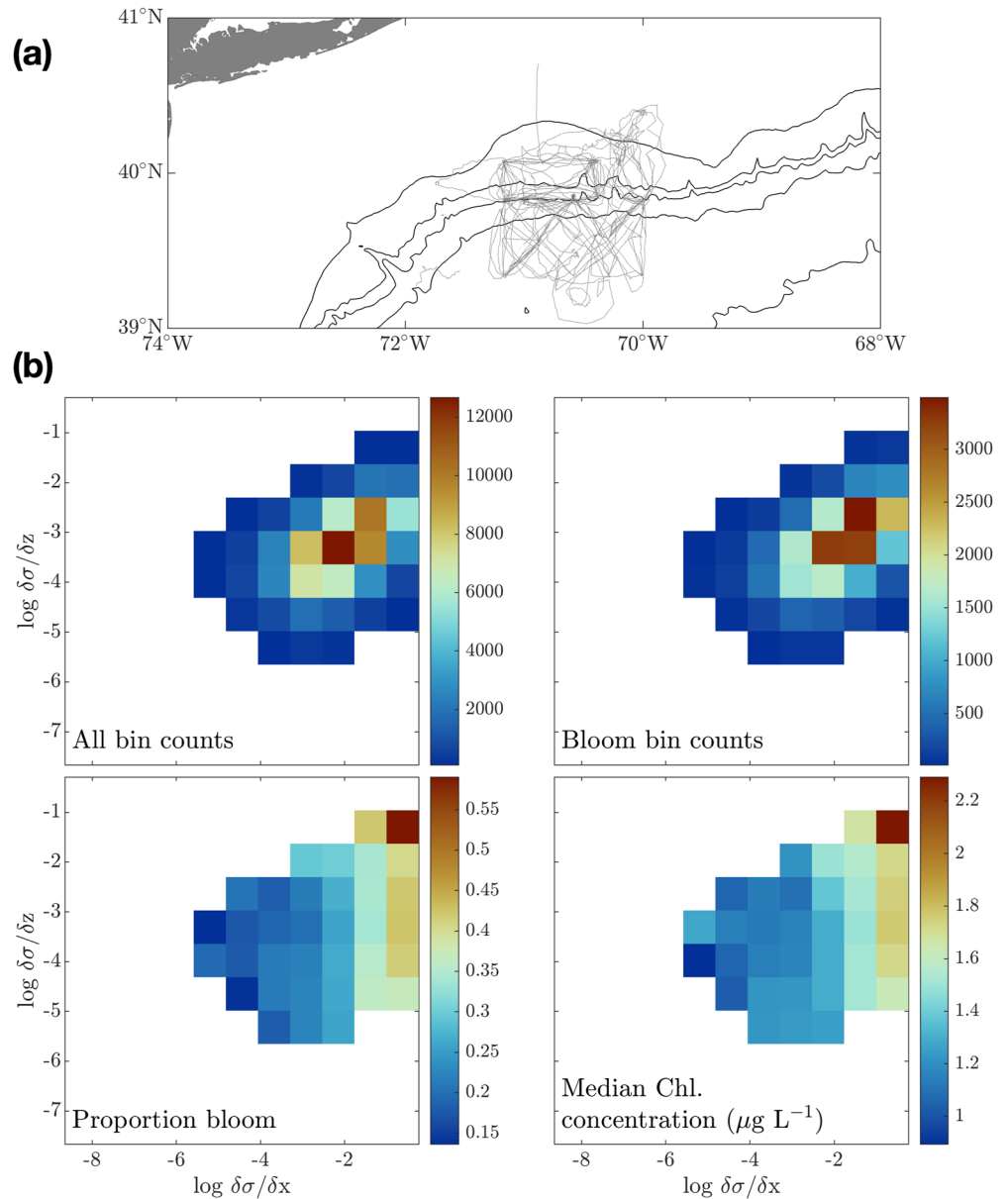


**Figure 10.** Ocean observatories initiative (OOI) Coastal Pioneer Array glider data from 2014–2020. (a) All April glider tracks; (b) OOI April glider chlorophyll, binned by horizontal and vertical stratification. The axis limits extend to bins where there was at least one observation; bins are only colored where there were at least 100 observations. Note the log-log axis scales.

opposes the surface frontal current, or upfront (eastward) winds (e.g., Long et al., 2012). To determine whether Ekman restratification is a likely driver for enhanced surface shelf-break chlorophyll for other periods, we explore whether upfront winds (from ERA5 reanalysis, Section 2.4) typically occur shortly before the “enhancement days” identified with ocean color data (Section 3.1).

Using 10-m  $u$  (zonal) and  $v$  (meridional) ERA5 wind speeds over the same grid points identified as corresponding to the shelf break for the ocean color analysis in Section 2.1, we compared the wind “upwelling index” ( $UI = \tau_x/\rho f$ , in  $\text{m}^2 \text{s}^{-1}$ ) with the timing of the shelf-break chlorophyll enhancement days identified in Section 3.1. The upwelling index is a measure of upfront vs. downfront winds (as calculated in Li et al., 2020), with  $\tau_x$  being the  $u$  component of the wind stress,  $\rho$  the water density, and  $f$  the Coriolis parameter. As most of the shelf break in our MODIS region is approximately zonally oriented, we use positive (negative)  $u$  wind stress as the upfront

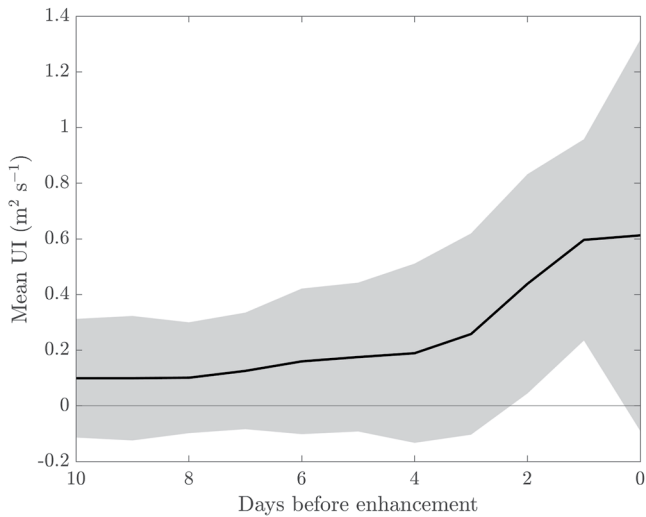


**Figure 11.** The mean ( $\pm$ standard deviation) upwelling index for  $n$  days leading up to first shelf-break surface chlorophyll enhancement.

(downfront) wind stress. We computed the average upwelling index for the 10 days preceding the first day of the shelf-break chlorophyll enhancements.

Indeed, enhanced remotely sensed shelf-break chlorophyll concentrations tend to be preceded by increasing upfront winds (Figure 11). The mean upfront wind stress typically increases in the three days preceding the enhancements of chlorophyll at the shelf break, with the mean upwelling index one day before the frontal enhancement being significantly larger than 4 days before ( $t = 3.8$ , 95% confidence interval:  $0.17\text{--}0.65\text{ m}^2$ ,  $p < 0.01$ ). In contrast, the mean upwelling index over periods longer than four days preceding the enhancements are not statistically different from zero ( $t = 2.3$ ,  $p > 0.05$ ).

We then ran the 2-D model for two contrasting conditions: one with constant  $5\text{ m s}^{-1}$  down-front winds, and the other with constant  $5\text{ m s}^{-1}$  upfront winds. Our simple 2D ROMS model demonstrates that Ekman restratification could generate similar patterns of chlorophyll at the front compared to those observed during AR29. In the first 3 days of the upfront wind model run, the front restratifies, the mixed layer becomes shallow, and chlorophyll rapidly accumulates in the shallow, stratified mixed layer (Figure 12b). In contrast, in the downfront wind case, the advection of denser slope water over less dense shelf water drives convective overturning on the shelf side of the front and the water column becomes well-mixed (e.g., D'Asaro et al., 2011; Thomas &

Lee, 2005). As a consequence, frontal phytoplankton concentrations are lower than on the shelf or the slope, as phytoplankton are diluted with vertical mixing and growth rates remain low (Figure 12c). Nutrient concentrations were replete in both model cases (Figure S6 in Supporting Information S1).

#### 4. Discussion

We demonstrate here that frontal chlorophyll enhancements detected at the New England shelf break are transient features. Its development is triggered by the increase in stratification resulting from the Ekman advection of less dense shelf water over denser slope water (Figure 13). Nutrients were replete at the shelf break at the time of the spring surface frontal chlorophyll enhancement observed during AR29; suggesting it was driven by stratification, not nutrients. When light availability, rather than nutrient availability, is the dominant control on phytoplankton growth, the influence of surface mixing is likely to be of leading-order importance on the development of spring blooms (Hopkins et al., 2021). The patterns in density and chlorophyll measured by OOI gliders are consistent with the hypothesis that Ekman restratification triggers a transient chlorophyll enhancement at the front. This is consistent with the findings of Xu et al. (2011) that interannual variability in spring bloom magnitude is associated with factors controlling water column stability, which is supported with a model testing the sensitivity to removing wind forcing (Xu et al., 2013). Our findings also agree with Xu et al. (2020), who found that increased wind mixing can delay the onset of the outer shelf spring bloom in the MAB. Given the small window during which shelf-break chlorophyll enhancements occur, they are masked in seasonal climatologies, though they are detectable in the DRM climatology (Figure 5a).

While our DRM chlorophyll climatology does not fully capture the transient quality of the shelf-break chlorophyll enhancements, which last less than a week, it agrees well with other studies of MAB chlorophyll variability. It is consistent with Ryan, Yoder, Cornillon, et al. (1999), who found annual shelf-break chlorophyll enhancement during the spring transition from well-mixed to stratified conditions. The climatology also agrees with the findings of Hales et al. (2009), who showed that shelf-break chlorophyll enhancements were not present in June or August. The large-scale seasonal variability in shelf and slope chlorophyll concentrations also agrees well with other modeling and observational studies of MAB chlorophyll, exhibiting a clear fall-winter bloom on the shelf and spring bloom in the slope (Fennel et al., 2006; Hofmann et al., 2011; Ryan, Yoder, Cornillon, et al., 1999; Xu et al., 2011, 2020; Yoder et al., 2001, 2002).

The chlorophyll enhancements identified were short-lived and dominated by nanoplankton in 2018. Unlike these shelf-break enhancements, earlier-season blooms on the U.S. Northeast Shelf are dominated by large cells (Marrec et al., 2021). Though nitrate and silicate concentrations are replete at the front in April 2018, microplankton

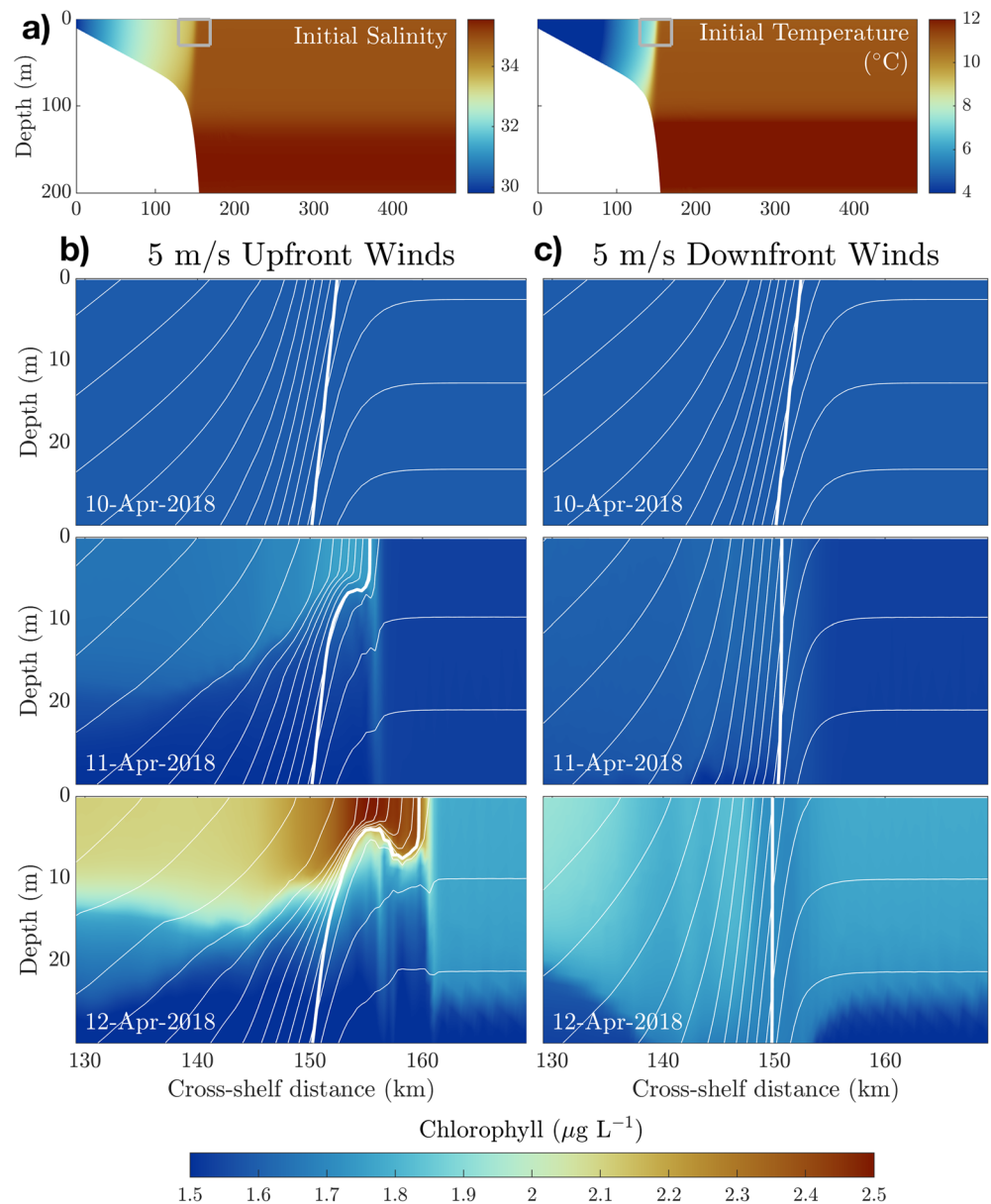


**Figure 12.** 2-D ROMS model initial condition and output. (a) Initial salinity and temperature, with the gray boxes showing the boundaries of the output fields shown in (b) and (c); (b) chlorophyll fields from 2-D ROMS model output with constant  $5 \text{ m s}^{-1}$  upfront winds; (c) output for constant  $5 \text{ m s}^{-1}$  downfront winds. The thick white lines show the frontal isohaline (34.5), and thinner white lines show isopycnals at  $0.05 \text{ kg m}^{-3}$  intervals. Chlorophyll is calculated from nitrogen units using the Redfield ratio (106 mol C:16 mol N; Redfield, 1963), and assuming 50 g C/g Chl.

biovolumes are not enhanced. The observed enhancement of microplankton biomass offshore of the front during AR29 was not associated with elevated chlorophyll (Figure 8g), and may have been associated with an earlier spring bloom on the slope, though elevated slope sea chlorophyll is not apparent in the satellite data (Figure 4). It is unknown why nanoplankton should outcompete diatoms at the front, though small phytoplankton have previously been observed to dominate phytoplankton assemblages on the restratified side of a front (Sangrà et al., 2014).

For upfront winds to drive a chlorophyll enhancement at the shelf break, the following conditions must hold: (a) nutrient concentrations must be replete at the surface, (b) the upper water column must initially be unstratified, and (c) the upfront winds must be strong enough to drive the movement of the front offshore, but not so strong to

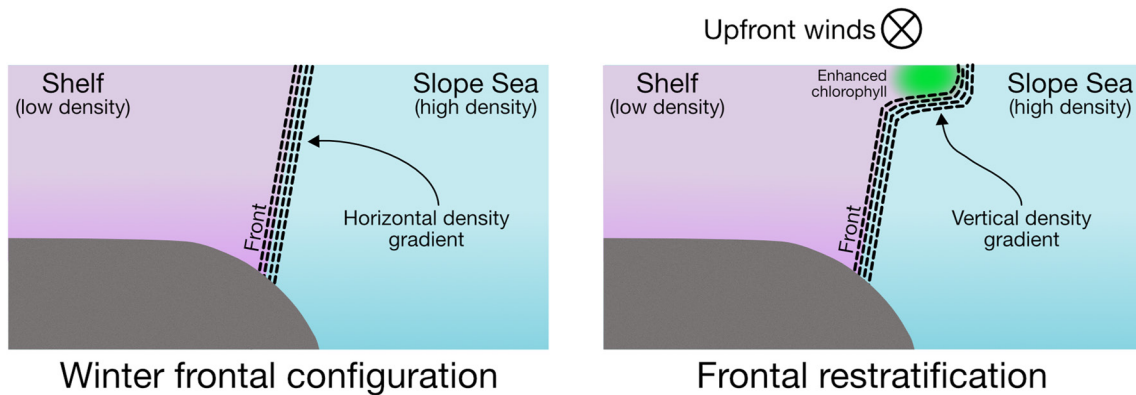


**Figure 13.** Conceptual diagram of an increasing vertical density gradient as isopycnals flatten with upfront winds, which creates a shallow, well-lit mixed layer that can support rapid phytoplankton accumulation.

deepen the mixed layer. This leaves only short periods during the year where these enhancements are possible. In addition to spring chlorophyll enhancements, transient autumn enhancements may also be possible with upfront winds occurring after the water column has destratified. Autumn enhancements were sometimes detected at the shelf break in our satellite chlorophyll analysis, for example in 2010, but did not appear in the chlorophyll climatology. While the mean winter winds in the MAB are also upfront, the upper water column remains well-mixed due to strong winds and buoyancy-driven mixing which prevent frontal slumping from occurring. The winter bloom on the inner shelf where the bottom is shallower suggests that there is still enough light in the region to allow phytoplankton to grow, presumably because the bottom depth restricts the extent of vertical mixing. The westerly winds weaken in the spring, although they continue to fluctuate substantially (Figure S1 in Supporting Information S1). The slumping may thus require intermediate westerly winds fluctuating on the time scale of days.

While Ekman restratification is an apparent trigger of enhanced surface chlorophyll at the shelf break, a variety of alternative restratifying dynamics are also possible. As strong horizontal density gradients adjust to geostrophic equilibrium (Ou, 1984), frontal restratification of the surface mixed layer can result (Tandon & Garrett, 1995). For example, frontal restratification can result from a reversal in wind direction (Dale et al., 2008) or from the rapid relaxation of winds (Johnson et al., 2020). In our analysis the presence of increasing upfront winds preceding surface shelf-break chlorophyll enhancements indicates Ekman restratification as the simplest explanation for the observed restratification.

Frontal eddies may also result in frontal restratification processes with the potential to initiate spring phytoplankton blooms, analogous to those found in the open ocean (Mahadevan et al., 2010, 2012). The New England shelf-break front is characterized by abundant eddy formation from frontal meandering (Garvine et al., 1988) that has been associated with enhanced chlorophyll (Ryan, Yoder, Barth, et al., 1999). While eddies may also play an additional role, our exploration of the relationship between shelf-break chlorophyll derived from MODIS-Aqua to surface wind forcing, and our 2-dimensional model runs suggest that upfront winds appear to be sufficient to drive the Ekman restratification required to stimulate shelf-break chlorophyll enhancements. Understanding potential 3-dimensional mechanisms involved with these enhancements will likely require exploring how chlorophyll corresponds to shelf-break eddy activity, which is beyond the scope of this 2-dimensional study.

This study aimed to understand the mechanisms driving surface chlorophyll enhancements observed at the shelf break, a conundrum in the literature. While the surface chlorophyll was our focus, subsurface enhancements of chlorophyll at the front have also been observed later in the growing season (e.g., Marra et al., 1990). Various upwelling mechanisms may still supply nutrients to the euphotic zone in the frontal region, supporting enhanced subsurface biological productivity (e.g., Friedrichs et al., 2019). Such upwelling mechanisms include frontal meandering (e.g., He et al., 2011), oscillating winds (Siedlecki et al., 2011), upwelling from the bottom boundary layer (Gawarkiewicz & Chapman, 1992), upwelling from the seaward side of the front (Zhang et al., 2013), and irregular topography (e.g., canyons; Hickey & Banas, 2008). The 2D-framework used in this study also does not preclude 3D-processes at the shelf break. In fact, it is likely that these 3D processes occur in addition to

the 2D-frontal restratification mechanism, resulting in along-shelf variability in the frontal surface chlorophyll enhancement.

## 5. Conclusions

The New England shelf break is thought to be highly productive in part due to enhanced chlorophyll detected at the shelf/slope front. Surface frontal enhancement is not discernible in seasonal climatologies (e.g., Zhang et al., 2013) although such enhancements are occasionally visible in synoptic images during spring. We demonstrate that frontal chlorophyll enhancement is an ephemeral process, typically lasting only a few days. We suggest that Ekman restratification driven by upfront winds results in the advection of the lighter shelf water over denser slope water. This process creates a shallow mixed layer at the front which alleviates light limitation and supports transient surface enhancements of chlorophyll at the front. Alternative submesoscale restratifying mechanisms are not precluded by our assessment, but the presence of intensified upfront winds preceding the shelf-break enhancements suggests Ekman restratification as the most straightforward explanation.

## Data Availability Statement

MODIS Aqua 8-Day 1 km composite chlorophyll concentrations were processed at the University of Delaware and can be accessed at [http://basin.ceoe.udel.edu/erddap/griddap/MODIS\\_AQUA\\_8\\_day.html](http://basin.ceoe.udel.edu/erddap/griddap/MODIS_AQUA_8_day.html). SPIROPA AR29 VPR Tow 1 and CTD Transect 5 data are archived at the Biological and Chemical Oceanography Data Management Office (BCO-DMO) project page: <https://www.bco-dmo.org/project/748894>. MAB historical nitrate and nitrate + nitrite data are available from the World Ocean Database provided by the National Centers for Environmental Information at the National Oceanic and Atmospheric Administration. OOI glider data, and 3 and 10 m wind speeds can be accessed at [https://ooinet.oceanobservatories.org/data\\_access/](https://ooinet.oceanobservatories.org/data_access/). ERA5 reanalysis wind speed data are available from the Copernicus Climate Change Service Climate Data Store (<https://cds.climate.copernicus.eu/cdsapp#!/dataset/reanalysis-era5-single-levels?tab=overview>).

## Acknowledgments

This research was supported by the National Science Foundation (OCE-1657803, OCE-1657855, and OCE-1655686) and the Dalio Explorer Fund. Support for H. Oliver was provided by the WHOI Postdoctoral Scholar program. We thank Jeff Turner and Chrissy Petipas for their work on higher trophic levels, Melissa Brennan and Josh Eaton for VPR operations, Taylor Crockford for IFCB operations, Emily Peacock for IFCB image classification, Zoe Sandwith for contributing to O<sub>2</sub>/Ar data collection and analysis, and our SPIROPA colleagues and crew of the R/V Neil Armstrong for their assistance and support at sea.

## References

- Anderson, L. A., & Sarmiento, J. L. (1994). Redfield ratios of remineralization determined by nutrient data analysis. *Global Biogeochemical Cycles*, 8(1), 65–80. <https://doi.org/10.1029/93GB03318>
- Chapman, D. C., & Lentz, S. J. (1994). Trapping of a coastal density front by the bottom boundary layer. *Journal of Physical Oceanography*, 24(7), 1464–1479. [https://doi.org/10.1175/1520-0485\(1994\)024<1464:toadf>2.0.co;2](https://doi.org/10.1175/1520-0485(1994)024<1464:toadf>2.0.co;2)
- Dale, A. C., Barth, J. A., Levine, M. D., & Austin, J. A. (2008). Observations of mixed layer restratification by onshore surface transport following wind reversal in a coastal upwelling region. *Journal of Geophysical Research*, 113(C1). <https://doi.org/10.1029/2007JC004128>
- D'Asaro, E., Lee, C., Rainville, L., Harcourt, R., & Thomas, L. (2011). Enhanced turbulence and energy dissipation at ocean fronts. *Science*, 332(6027), 318–322. <https://doi.org/10.1126/science.1201515>
- Davis, C. S., Thwaites, F. T., Gallagher, S. M., Hu, Q., Naiman, M., Sutton, T., et al. (2005). A three-axis fast-tow digital video plankton recorder for rapid surveys of plankton taxa and hydrography. *Limnology and Oceanography: Methods*, 3, 59–74. <https://doi.org/10.4319/lom.2005.3.59>
- Fennel, K., Wilkin, J., Levin, J., Moisan, J., O'Reilly, J., & Haidvogel, D. (2006). Nitrogen cycling in the Middle Atlantic Bight: Results from a three-dimensional model and implications for the North Atlantic nitrogen budget. *Global Biogeochemical Cycles*, 20(3), 1–14. <https://doi.org/10.1029/2005GB002456>
- Ferrari, R., Merrifield, S. T., & Taylor, J. R. (2015). Shutdown of convection triggers increase of surface chlorophyll. *Journal of Marine Systems*, 147, 116–122. <https://doi.org/10.1016/j.jmarsys.2014.02.009>
- Fratantoni, P. S. (2003). Variability of the shelf break jet in the Middle Atlantic Bight: Internally or externally forced? *Journal of Geophysical Research*, 108(C5), 3166. <https://doi.org/10.1029/2002JC001326>
- Friedrichs, M. A. M., St-Laurent, P., Xiao, Y., Hofmann, E., Hyde, K., Mannino, A., et al. (2019). Ocean circulation causes strong variability in the Mid-Atlantic Bight nitrogen budget. *Journal of Geophysical Research: Oceans*, 124(1), 113–134. <https://doi.org/10.1029/2018JC014424>
- Garcia, H., Weathers, K. W., Paver, C. R., Smolyar, I., Boyer, T. P., Locarnini, R. A., et al. (2019). World Ocean Atlas 2018. Vol. 4: Dissolved inorganic nutrients (phosphate, nitrate and nitrate+nitrite, silicate). *NOAA Atlas NESDIS*, 82, 35.
- Garvine, R. W., Wong, K.-C., Gawarkiewicz, G. G., McCarthy, R. K., Houghton, R. W., & Aikman, F. (1988). The morphology of shelfbreak eddies. *Journal of Geophysical Research*, 93(C12), 15593. <https://doi.org/10.1029/JC093iC12p15593>
- Gawarkiewicz, G., & Chapman, D. C. (1992). The role of stratification in the formation and maintenance of shelf-break fronts. *Journal of Physical Oceanography*, 22(7), 753–772. [https://doi.org/10.1175/1520-0485\(1992\)022<0753:trosit>2.0.co;2](https://doi.org/10.1175/1520-0485(1992)022<0753:trosit>2.0.co;2)
- Gawarkiewicz, G., & Plueddemann, A. J. (2020). Scientific rationale and conceptual design of a process-oriented shelfbreak observatory: The OOI pioneer array. *Journal of Operational Oceanography*, 13(1), 19–36. <https://doi.org/10.1080/1755876X.2019.1679609>
- Hales, B., Vaillancourt, R. D., Prieto, L., Marra, J., Houghton, R., & Hebert, D. (2009). High-resolution surveys of the biogeochemistry of the New England shelfbreak front during Summer, 2002. *Journal of Marine Systems*, 78(3), 426–441. <https://doi.org/10.1016/j.jmarsys.2008.11.024>
- He, R., Chen, K., Fennel, K., Gawarkiewicz, G. G., & McGillicuddy, D. J. (2011). Seasonal and interannual variability of physical and biological dynamics at the shelfbreak front of the Middle Atlantic Bight: Nutrient supply mechanisms. *Biogeosciences*, 8(10), 2935–2946. <https://doi.org/10.5194/bg-8-2935-2011>

- Hersbach, H., Bell, B., Berrisford, P., Biavati, G., Horányi, A., Muñoz Sabater, J., et al. (2018). *ERA5 hourly data on single levels from 1979 to present*. Copernicus climate change service (C3S) Climate data store (CDS). <https://doi.org/10.24381/cds.adbb2d47>
- Hickey, B., & Banas, N. (2008). Why is the Northern end of the California current system so productive? *Oceanography*, 21(4), 90–107. <https://doi.org/10.5670/oceanog.2008.07>
- Hofmann, E. E., Cahill, B., Fennel, K., Friedrichs, M. A. M., Hyde, K., Lee, C., et al. (2011). Modeling the dynamics of continental shelf carbon. *Annual Review of Marine Science*, 3(1), 93–122. <https://doi.org/10.1146/annurev-marine-120709-142740>
- Hopkins, J. E., Palmer, M. R., Poulton, A. J., Hickman, A. E., & Sharples, J. (2021). Control of a phytoplankton bloom by wind-driven vertical mixing and light availability. *Limnology and Oceanography* (1953), 1–24. <https://doi.org/10.1002/lno.11734>
- Johnson, L., Lee, C. M., D'Asaro, E. A., Wenegeat, J. O., & Thomas, L. N. (2020). Restratification at a California current upwelling front. Part II: Dynamics. *Journal of Physical Oceanography*, 50(5), 1473–1487. <https://doi.org/10.1175/JPO-D-19-0204.1>
- Li, Y., Stumpf, R. P., McGillicuddy, D. J., & He, R. (2020). Dynamics of an intense *Alexandrium catenella* red tide in the Gulf of Maine: Satellite observations and numerical modeling. *Harmful Algae*, 99, 101927. <https://doi.org/10.1016/j.hal.2020.101927>
- Linder, C. A., & Gawarkiewicz, G. (1998). A climatology of the shelfbreak front in the Middle Atlantic Bight. *Journal of Geophysical Research*, 103(C9). <https://doi.org/10.1029/98JC01438>
- Linder, C. A., Gawarkiewicz, G. G., & Pickart, R. S. (2004). Seasonal characteristics of bottom boundary layer detachment at the shelfbreak front in the Middle Atlantic Bight. *Journal of Geophysical Research*, 109(3), 1–9. <https://doi.org/10.1029/2003JC002032>
- Long, M. C., Thomas, L. N., & Dunbar, R. B. (2012). Control of phytoplankton bloom inception in the Ross Sea, Antarctica, by Ekman restratification. *Global Biogeochemical Cycles*, 26(1), 1–14. <https://doi.org/10.1029/2010GB003982>
- Lozier, M. S., & Reed, M. S. C. (2005). The influence of topography on the stability of shelfbreak fronts. *Journal of Physical Oceanography*, 35(6), 1023–1036. <https://doi.org/10.1175/JPO2717.1>
- Mahadevan, A., D'Asaro, E., Lee, C., & Perry, M. J. (2012). Eddy-driven stratification initiates North Atlantic spring phytoplankton blooms. *Science*, 337(6090), 54–58. <https://doi.org/10.1126/science.1218740>
- Mahadevan, A., Tandon, A., & Ferrari, R. (2010). Rapid changes in mixed layer stratification driven by submesoscale instabilities and winds. *Journal of Geophysical Research*, 115(3), 1–12. <https://doi.org/10.1029/2008JC005203>
- Marra, J., Houghton, R. W., Boardman, D. C., & Neale, P. J. (1982). Variability in surface chlorophyll a at a shelf-break front. *Journal of Marine Research*, 40(3), 575–591.
- Marra, J., Houghton, R. W., & Garside, C. (1990). Phytoplankton growth at the shelf-break front in the Middle Atlantic Bight. *Journal of Marine Research*, 48(4), 851–868. <https://doi.org/10.1357/002224090784988665>
- Marrec, P., McNair, H., Franzè, G., Morison, F., Strock, J. P., & Menden-Deuer, S. (2021). Seasonal variability in planktonic food web structure and function of the Northeast U.S. Shelf. *Limnology and Oceanography*, 1440–1458. <https://doi.org/10.1002/lno.11696>
- Moberg, E. A., & Sosik, H. M. (2012). Distance maps to estimate cell volume from two-dimensional plankton images. *Limnology and Oceanography: Methods*, 10(4), 278–288. <https://doi.org/10.4319/lom.2012.10.278>
- O'Reilly, J. E., & Busch, D. A. (1984). Phytoplankton primary production on the Northwestern Atlantic shelf. *Rapports et Proces-Verbaux Des Reunions*, 183, 255–268.
- O'Reilly, J. E., Evans-Zetlin, C., & Busch, D. A. (1987). Primary production. In R. H. Backus, & D. W. Bourne (Eds.), *Georges bank* (pp. 220–233). MIT Press.
- Orphanides, C. D., & Magnusson, G. M. (2007). *Characterization of the Northeast and Mid-Atlantic bottom and mid-water trawl fisheries based on vessel trip report (VTR) data, northeast fisheries. Science center reference documents report 07-15*. (pp. 127). National Marine Fisheries Service, NOAA, U.S. Department of Commerce.
- Ou, H. W. (1984). Geostrophic adjustment: A mechanism for frontogenesis. *Journal of Physical Oceanography*, 14(6), 9942–1000. [https://doi.org/10.1175/1520-0485\(1984\)014<0994:gaamff>2.0.co;2](https://doi.org/10.1175/1520-0485(1984)014<0994:gaamff>2.0.co;2)
- Podestá, G. P., Browder, J. A., & Hoey, J. J. (1993). Exploring the association between swordfish catch rates and thermal fronts on U.S. longline grounds in the western North Atlantic. *Continental Shelf Research*, 13(2–3), 253–277. [https://doi.org/10.1016/0278-4343\(93\)90109-B](https://doi.org/10.1016/0278-4343(93)90109-B)
- Powell, T. M., Lewis, C. V. W. W., Curchitser, E. N., Haidvogel, D. B., Hermann, A. J., & Dobbins, E. L. (2006). Results from a three-dimensional, nested biological-physical model of the California Current System and comparisons with statistics from satellite imagery. *Journal of Geophysical Research*, 111(7), 1–14. <https://doi.org/10.1029/2004JC002506>
- Redfield, A. C. (1963). The influence of organisms on the composition of sea-water. *The Sea*, 26–77.
- Ryan, J. P., Yoder, J. A., Barth, J. A., & Cornillon, P. C. (1999). Chlorophyll enhancement and mixing associated with meanders of the shelf break front in the Mid-Atlantic Bight. *Journal of Geophysical Research*, 104(C10), 23479–23493. <https://doi.org/10.1029/1999jc900174>
- Ryan, J. P., Yoder, J. A., & Cornillon, P. C. (1999). Enhanced chlorophyll at the shelfbreak of the mid-Atlantic Bight and Georges bank during the spring transition. *Limnology and Oceanography*, 44(1), 1–11. <https://doi.org/10.4319/lno.1999.44.1.0001>
- Sangrà, P., García-Muñoz, C., García, C. M., Marrero-Díaz, Á., Sobrino, C., Mouriño-Carballido, B., et al. (2014). Coupling between upper ocean layer variability and size-fractionated phytoplankton in a non-nutrient-limited environment. *Marine Ecology Progress Series*, 499, 35–46. <https://doi.org/10.3354/meps10668>
- Shchepetkin, A. F., & McWilliams, J. C. (2005). The regional oceanic modeling system (ROMS): A split-explicit, free-surface, topography-following-coordinate oceanic model. *Ocean Modelling*, 9(4), 347–404. <https://doi.org/10.1016/j.ocemod.2004.08.002>
- Sherman, K., Jaworski, N. A., & Smayda, T. J. (1996). *The Northeast Shelf ecosystem: Assessment, sustainability and management*. Blackwell Science, Inc.
- Siedlecki, S. A., Archer, D. E., & Mahadevan, A. (2011). Nutrient exchange and ventilation of benthic gases across the continental shelf break. *Journal of Geophysical Research*, 116(6), 1–15. <https://doi.org/10.1029/2010JC006365>
- Smith, W. O., Zhang, W. G., Hirzel, A., Stanley, R. M., Meyer, M. G., Sosik, H., et al. (2021). A regional, early spring bloom of *Phaeocystis pouchetii* on the New England continental shelf. *Journal of Geophysical Research: Oceans*, 126(2), 2020JC016856. <https://doi.org/10.1029/2020JC016856>
- Sosik, H. M., & Olson, R. J. (2007). Automated taxonomic classification of phytoplankton sampled with imaging-in-flow cytometry. *Limnology and Oceanography: Methods*, 5(6), 204–216. <https://doi.org/10.4319/lom.2007.5.204>
- Sosik, H. M., Peacock, E., & Santos, M. (2020). *Abundance and biovolume of taxonomically-resolved phytoplankton and microzooplankton imaged continuously underway with an Imaging FlowCytobot along the NES-LTER Transect in winter 2018 ver 1*. Environmental Data Initiative. <https://doi.org/10.6073/pasta/74775c4af51c237f2a20e4a8c011bc53>
- Sverdrup, H. U. (1953). On conditions for the vernal blooming of phytoplankton. *ICES Journal of Marine Science*, 18(3), 287–295. <https://doi.org/10.1093/icesjms/18.3.287>
- Tandon, A., & Garrett, C. (1995). Geostrophic adjustment and restratification of a mixed layer with horizontal gradients above a stratified layer. *Journal of Physical Oceanography*, 25(10), 2229–2241. [https://doi.org/10.1175/1520-0485\(1995\)025<2229:gaaroa>2.0.co;2](https://doi.org/10.1175/1520-0485(1995)025<2229:gaaroa>2.0.co;2)



- Taylor, J. R., & Ferrari, R. (2011). Shutdown of turbulent convection as a new criterion for the onset of spring phytoplankton blooms. *Limnology and Oceanography*, *56*(6), 2293–2307. <https://doi.org/10.4319/lo.2011.56.6.2293>
- Thomas, L. N., & Lee, C. M. (2005). Intensification of ocean fronts by down-front winds. *Journal of Physical Oceanography*, *35*(6), 1086–1102. <https://doi.org/10.1175/JPO2737.1>
- Townsend, D. W., Keller, M. D., Sieracki, M. E., & Ackleson, S. G. (1992). Spring phytoplankton blooms in the absence of vertical water column stratification. *Nature*, *360*(6399), 59–62. <https://doi.org/10.1038/360059a0>
- Trowbridge, J., Weller, R., Kelley, D., Dever, E., Plueddemann, A., Barth, J. A., et al. (2019). The ocean observatories initiative. *Frontiers in Marine Science*, *6*, 1–23. <https://doi.org/10.3389/fmars.2019.00074>
- Xu, Y., Cahill, B., Wilkin, J., & Schofield, O. (2013). Role of wind in regulating phytoplankton blooms on the Mid-Atlantic Bight. *Continental Shelf Research*, *63*, 26–35. <https://doi.org/10.1016/j.csr.2012.09.011>
- Xu, Y., Chant, R., Gong, D., Castelao, R., Glenn, S., & Schofield, O. (2011). Seasonal variability of chlorophyll a in the mid-Atlantic Bight. *Continental Shelf Research*, *31*(16), 1640–1650. <https://doi.org/10.1016/j.csr.2011.05.019>
- Xu, Y., Miles, T., & Schofield, O. (2020). Physical processes controlling chlorophyll-a variability on the Mid-Atlantic Bight along Northeast United States. *Journal of Marine Systems*, *212*. <https://doi.org/10.1016/j.jmarsys.2020.103433>
- Yoder, J. A., O'Reilly, J. E., Barnard, A. H., Moore, T. S., & Ruhsam, C. M. (2001). Variability in coastal zone color scanner (CZCS) chlorophyll imagery of ocean margin waters off the US East Coast. *Continental Shelf Research*, *21*(11–12), 1191–1218. [https://doi.org/10.1016/S0278-4343\(01\)00009-7](https://doi.org/10.1016/S0278-4343(01)00009-7)
- Yoder, J. A., Schollaert, S. E., & O'Reilly, J. E. (2002). Climatological phytoplankton chlorophyll and sea surface temperature patterns in continental shelf and slope waters off the northeast U.S. coast. *Limnology and Oceanography*, *47*(3), 672–682. <https://doi.org/10.4319/lo.2002.47.3.0672>
- Zhang, W. G., & Gawarkiewicz, G. G. (2015). Length scale of the finite-amplitude meanders of Shelfbreak Fronts. *Journal of Physical Oceanography*, *45*(10), 2598–2620. <https://doi.org/10.1175/JPO-D-14-0249.1>
- Zhang, W. G., Gawarkiewicz, G. G., McGillicuddy, D. J., & Wilkin, J. L. (2011). Climatological mean circulation at the New England shelf break. *Journal of Physical Oceanography*, *41*(10), 1874–1893. <https://doi.org/10.1175/2011JPO4604.1>
- Zhang, W. G., McGillicuddy, D. J., & Gawarkiewicz, G. G. (2013). Is biological productivity enhanced at the New England shelfbreak front? *Journal of Geophysical Research: Oceans*, *118*(1), 517–535. <https://doi.org/10.1002/jgrc.20068>